Titre: Title:	Three-dimensional closure of the passage-averaged vorticity-potential formulation
Auteurs: Authors:	Xudong Zhang, André Garon, & Ricardo Camarero
Date:	1992
Type:	Rapport / Report
Référence: Citation:	Zhang, X., Garon, A., & Camarero, R. (1992). Three-dimensional closure of the passage-averaged vorticity-potential formulation. (Technical Report n° EPM-RT-92-05). https://publications.polymtl.ca/10148/

Institution:	École Polytechnique de Montréal
Numéro de rapport: Report number:	EPM-RT-92-05
URL officiel: Official URL:	
Mention légale: Legal notice:	

EPM/RT-92-5

THREE-DIMENSIONAL CLOSURE OF THE PASSAGE-AVERAGED VORTICITY-POTENTIAL FORMULATION

Xudong Zhang, Research Assistant
André Garon, Research Fellow
Ricardo Camarero, Professor

Génie Mécanique

École Polytechnique de Montréal
avril 1992

Ce document a pu être publié grâce à une subvention du Conseil de recherches en sciences et en génie du Canada (CRSNG)

Dépôt légal, 2e trimestre 1992
Bibliothèque nationale du Québec
Bibliothèque nationale du Canada

Pour se procurer une copie de ce document, s'adresser au:

Service de l'édition
École Polytechnique de Montréal
Case postale 6079, Succursale A
Montréal (Québec) H3C 3A7
(514) 340-4000

Compter 0,10$ par page (arrondir au dollar le plus près) et ajouter 3,00$ (Canada) pour la couverture, les frais de poste et la manutention. Régler en dollars canadiens par chèque ou mandat-poste au nom de l'École Polytechnique de Montréal. Nous n'honorerons que les commandes accompagnées d'un paiement, sauf s'il y a eu entente préalable dans le cas d'établissements d'enseignement, de sociétés ou d'organismes canadiens.

THREE-DIMENSIONAL CLOSURE OF THE PASSAGE-AVERAGED VORTICITY-POTENTIAL FORMULATION

Xudong Zhang*, André Garon†, Ricardo Camarero‡
École Polytechnique de Montréal, C.P. 6079, Succ. A,
Montréal, Québec, Canada, H3C 3A7

Abstract

The closure model of a passage-averaged vorticity-potential formulation of the governing equations for simulation of viscous flow in a rotor-stator stage of a turbomachine is presented. In the passage-averaged equations, the presence of the blades is accounted for by force terms whose values are deduced from the three-dimensional flow fields. This procedure requires some iterations between the passage-averaged solutions and the three-dimensional solutions to achieve a convergent flow field. To demonstrate their capability to predict complex turbomachinery flows, comparison of the numerical results with experimental data for a mixed-flow pump are presented.

*Research Assistant

†Research Fellow

‡Professor

1 Introduction

The numerical simulation of the fluid dynamics in turbomachines is a difficult subject due to complex three-dimensional viscous effects, further complicated by rotor-stator flow interactions. Because the flow field is unsteady, spatially aperiodic and highly rotational. The coupling between the stator and rotor flows in a turbomachine is an extremely difficult problem for which direct simulation of viscous flow is still not practical within current computational capabilities. Thus a reduction of the complexity, based on a simplification of the governing set of equations by appropriate modelling and approximations, is a sensible strategy.

In an effort to model the rotor-stator interaction, the through-flow approximation has played an important role. In simulating flows in multistage turbomachines, there are in general two types of through-flow approximations. The first one is the streamsurface technique and the second is the passage-averaged technique.

The development of the streamsurface technique can be traced back to the work of Wu [1] in which the conservation equations are expressed directly on the volume enclosed between two streamsurfaces with a given circumferential thickness. Both the streamsurface and the thickness are flow dependent and have to be determined by blade-to-blade calculations. Three-dimensional calculations is performed by iteratively computing the two families of intersecting streamsurfaces ([2] and [3]). In the quasi-three-dimensional approximation, it is assumed that the blade-to-blade S_1 surfaces are surfaces of revolution and only one hub-to-shroud S_2 surface is used ([3] and [4])

The passage-averaged representation is obtained by integrating the flow equations in the circumferential direction of the blade row. This means that the passage-averaged flow properties are defined on the meridional cross-section of the turbomachine. If the flow is assumed to be periodic from one blade

passage to another, the passage-averaged flow properties can be represented by integration from the pressure side to suction side of the blade. In the derived formulations, a tangential blockage parameter, which is a geometrical factor, is introduced to replace the flow dependent streamsheet thickness in the stream-surface formulations.

In this class of approximation the blade-to-blade effects are replaced by external forces which are coupled to the through-flow governing equations. To evaluate these external forces, a closure model must be developed. This approach was initially proposed by [5] for applications in through-flow calculations and subsequently used by [6] and [4].

Most of these methods have been used effectively to deal with the inviscid flow through turbomachines and can be credited with many interesting results to both analysis and design problems. A more complete three-dimensional average-passage equation system has been developed by [7], especially derived for analyzing viscous flows in multistage turbomachines. Its applications include the calculation of the inviscid flow through a counterrotating propeller [8,9] and the simulation of the viscous flow in an axial flow turbine [10].

The objectives of this paper are, taking advantage of the passage-averaged through-flow approximation and the vorticity-potential representation of the Navier-Stokes equations, to develop a numerical algorithm for the prediction of a rotor-stator flow interaction.

The closure model in obtained by passage-averaging the vorticity-potential formulation of the Navier-Stokes equations and the resulting external forces are calculated from three-dimensional solutions within blade rows instead of an approximate blade-to-blade solutions or correlations. Furthermore an algorithm has been developed to solve the passage-averaged equations and an implicit algorithm has been developed for the three-dimensional predictions within blade

rows.

2 Governing Equations

Vorticity-Potential Equations (3D)

The main difficulties related to the computation of incompressible flows is that the momentum equations must be solved subject to the continuity constraint. In two dimensions the vorticity-stream function method [14] is frequently used to overcome this difficulty. In such a formulation, the pressure is eliminated by cross differentiation over the momentum equations which yields a vorticity transport equation.

In three dimensions, the pressure is also removed by cross differentiation of the momentum equations, but the introduction of the stream function is not straightforward. One approach is to replace the velocity by the vorticity and vector potentials. The reduced equations then involve three vorticity transport equations and three equations governing the vector potential components (see [15])

The basic principle behind the scalar-vector potential method is the splitting of the velocity field $\mathbf{V} = (v^r, v^\theta, v^z)$, where (r, θ, z) is the cylindrical coordinates, into its rotational and irrotational parts based on Helmholtz's decomposition theorem, i.e.

$$\mathbf{V} = -\nabla\phi + \nabla \times \mathbf{A} \tag{1}$$

where ϕ is a scalar potential field satisfying the Laplace equation and $\mathbf{A} = (A^r, A^\theta, A^z)$ is a solenoidal(or divergence free) vector potential field.

Clearly, equation (1) ensures that the continuity equation is automatically satisfied. Then the complete set of the three-dimensional governing equations

(3DGE) can be written as follows

$$(\mathbf{V}\cdot\nabla)\mathbf{W} - (\mathbf{W}\cdot\nabla)\mathbf{V} = \frac{1}{Re}\nabla^2\mathbf{W} \tag{2}$$

$$\nabla^2\phi = 0 \tag{3}$$

$$\nabla^2\mathbf{A} = -\mathbf{W} \tag{4}$$

$$\mathbf{V} = -\nabla\phi + \nabla\times\mathbf{A} \tag{5}$$

where $\mathbf{W} = (w^r,\ w^\theta,\ w^z)$ is the vorticity field and Re is the Reynolds number.

Passage-Averaging Operator

Assuming a periodic flow field within a blade row, the passage-averaged operator for any quantity q is defined as

$$\overline{q} = \frac{1}{\delta}\int_{\theta}^{\theta} q\,d\theta \tag{6}$$

where $\delta = \theta_s - \theta_p$ within a single blade passage. Here θ_p and θ_s are simply the equations of the pressure and suction surfaces, respectively, of the blade passage defined by the following representations

$$\lambda_s(r,\theta,z) = \theta - \theta_s(r,z) = 0 \tag{7}$$

$$\lambda_p(r,\theta,z) = \theta - \theta_p(r,z) = 0 \tag{8}$$

$$\lambda_c(r,\theta,z) = \theta - \theta_c(r,z) = 0 \tag{9}$$

where θ_c is the equation of the camber surface.

The gradients of the pressure surface and the suction surfaces are related to the gradient of the camber surface by the following equations

$$\nabla\lambda_s = \nabla\lambda_c - \frac{k}{2}\nabla B \tag{10}$$

$$\nabla\lambda_p = \nabla\lambda_c + \frac{k}{2}\nabla B \tag{11}$$

where $k = 2\pi/N$ is the maximum angular aperture of a blade-passage, in which N represents the blade number, and B is the ratio of the actual angular aperture to k, i.e.

$$B = \frac{\delta}{k} \tag{12}$$

With the help of these definitions and Leibniz' rule, one can show that the passage-averaged form of the derivative of a function q is given by

$$\overline{\frac{\partial q}{\partial x^i}} = \frac{1}{B}\frac{\partial(B\overline{q})}{\partial x^i} + \frac{1}{\delta}[q_s\frac{\partial \lambda_s}{\partial x^i} - q_p\frac{\partial \lambda_p}{\partial x^i}] \tag{13}$$

From which it is possible to derive the following formulas

$$\overline{\nabla q} = \frac{1}{B}\nabla(B\overline{q}) + \frac{1}{\delta}[q_s\nabla\lambda_s - q_p\nabla\lambda_p] \tag{14}$$

$$\overline{\nabla\cdot\mathbf{V}} = \frac{1}{B}\nabla\cdot(B\overline{\mathbf{V}}) + \frac{1}{\delta}[\mathbf{V}_s\cdot\nabla\lambda_s - \mathbf{V}_p\cdot\nabla\lambda_p] \tag{15}$$

$$\overline{\nabla\times\mathbf{V}} = \frac{1}{B}\nabla\times(B\overline{\mathbf{V}}) + \frac{1}{\delta}[\nabla\lambda_s\times\mathbf{V}_s - \nabla\lambda_p\times\mathbf{V}_p] \tag{16}$$

needed to arrive at the passage-averaged equations described in the following section. Where subscripts "s" and "p" represent the values of the variables on the suction surface and pressure surface respectively.

Passage-Averaged Equations

The three-dimensional equations (2–5) are passage-averaged and the resulting set of equations are written as follows

$$(\overline{\mathbf{V}}\cdot\nabla)(B\overline{\mathbf{W}}) - (B\overline{\mathbf{W}}\cdot\nabla)\overline{\mathbf{V}} = \frac{1}{Re}\nabla^2(B\overline{\mathbf{W}}) + \mathbf{F}_W \tag{17}$$

$$\nabla^2(B\overline{\phi}) = F_\phi \tag{18}$$

$$\nabla^2(B\overline{\mathbf{A}}) = -B\overline{\mathbf{W}} + \mathbf{F}_A \tag{19}$$

$$B\overline{\mathbf{V}} = -\nabla(B\overline{\phi}) + \nabla\times(B\overline{\mathbf{A}}) + \mathbf{F}_V \tag{20}$$

These equations have been obtained using equation (14–16) and the fact that the Laplacian of the velocity field can be written as the product of the divergence of the velocity field and the rotational of the vorticity.

In these equations, external force terms appear as a result of the passage-averaging operator. For completeness, they are

$$\begin{aligned}
\mathbf{F}_W = \frac{1}{Re\ k}\{ & \quad [\nabla(\mathbf{W}_s \cdot \nabla\lambda_s) - \nabla(\mathbf{W}_p \cdot \nabla\lambda_p)] \\
& - [\nabla \times (\nabla\lambda_s \times \mathbf{W}_s) - \nabla \times (\nabla\lambda_p \times \mathbf{W}_p)] \\
& - [\nabla\lambda_s \times (\nabla \times \mathbf{W})_s - \nabla\lambda_p \times (\nabla \times \mathbf{W})_p]\} \\
- \frac{1}{k}\{ & \quad \bar{\mathbf{V}}[\mathbf{W}_s \cdot \nabla\lambda_s - \mathbf{W}_p \cdot \nabla\lambda_p] \\
& + [\nabla\lambda_s \times (\mathbf{W} \times \mathbf{V}_\Omega)_s - \nabla\lambda_p \times (\mathbf{W} \times \mathbf{V}_\Omega)_p]\} \\
& - [\nabla \times (B\overline{\tilde{\mathbf{W}} \times \tilde{\mathbf{V}}}) + \bar{\mathbf{W}}(\nabla B \cdot \bar{\mathbf{V}})] \qquad (21)
\end{aligned}$$

$$\mathbf{F}_V = -\frac{1}{k}[\phi_s \nabla\lambda_s - \phi_p \nabla\lambda_p] \qquad (22)$$

$$F_\phi = \nabla \cdot \mathbf{F}_V \qquad (23)$$

$$\begin{aligned}
\mathbf{F}_A = & -\nabla(\mathbf{A}_s \cdot \nabla\lambda_s - \mathbf{A}_p \cdot \nabla\lambda_p) \\
& -\frac{1}{k}[\nabla\lambda_s \times (\nabla \times \mathbf{A})_s - \nabla\lambda_p \times (\nabla \times \mathbf{A})_p] \qquad (24)
\end{aligned}$$

where the tilde " ~ " represents their perturbation from their average value. These perturbation terms are not necessarily small, and indeed they are not assumed to be small in this development.

Modified Passage-Averaged Equations

In the passage-averaged equations, $\bar{A}^r$ and $\bar{A}^z$ components of the vector potential, and, $\bar{w}^r$ and $\bar{w}^z$ components of the vorticity are used to compute the circumferential velocity $\bar{v}^\theta$. However, these four variables are unnecessary if we introduce $\bar{v}^\theta$ passage-averaged momentum equation. Then, the modified passage-averaged governing equations (MPAGE) are

$$\begin{aligned}
\bar{v}^r \frac{\partial}{\partial r}(B\bar{w}^\theta) + \bar{v}^z \frac{\partial}{\partial z}(B\bar{w}^\theta) - \frac{\bar{v}^r}{r}(B\bar{w}^\theta) - \frac{1}{r}\frac{\partial}{\partial z}(B\bar{v}^\theta\bar{v}^\theta) \\
= \frac{1}{Re}\{\frac{\partial}{\partial r}[\frac{1}{r}\frac{\partial}{\partial r}(rB\bar{w}^\theta)] + \frac{\partial^2}{\partial z^2}(B\bar{w}^\theta)\} + F_w^\theta \qquad (25)
\end{aligned}$$

$$\frac{1}{r}\frac{\partial}{\partial r}[r\frac{\partial}{\partial r}(B\bar{\phi})] + \frac{\partial^2}{\partial z^2}(B\bar{\phi}) = F_\phi \tag{26}$$

$$\frac{\partial}{\partial r}[\frac{1}{r}\frac{\partial}{\partial r}(B\bar{A}^\theta)] + \frac{\partial^2}{\partial z^2}(B\bar{A}^\theta) = -B\bar{W}^\theta + F_A^\theta \tag{27}$$

$$\bar{v}^r\frac{\partial}{\partial r}(B\bar{v}^\theta) + \bar{v}^z\frac{\partial}{\partial z}(B\bar{v}^\theta) + \frac{\bar{v}^r}{r}(B\bar{v}^\theta) = \frac{1}{Re}\{\frac{\partial}{\partial r}[\frac{1}{r}\frac{\partial}{\partial r}(rB\bar{v}^\theta)] + \frac{\partial^2}{\partial z^2}(B\bar{v}^\theta)\} + F_v^\theta \tag{28}$$

where

$$B\bar{v}^r = -\frac{\partial B\bar{\phi}}{\partial r} - \frac{\partial(B\bar{A}^\theta)}{\partial z} + F_v^r \tag{29}$$

$$B\bar{v}^z = -\frac{\partial B\bar{\phi}}{\partial z} + \frac{\partial(B\bar{A}^\theta)}{\partial r} + \frac{1}{r}(B\bar{A}^\theta) + F_v^z \tag{30}$$

and F_w^θ, F_ϕ, F_A^θ, F_v^θ, F_v^r and F_v^z are external forces detailed in Appendix. Equations (25–27, 29–30) are obtained directly from the passage-averaged equations (17–20), and equations (28) is the passage-averaged momentum equation for $\bar{v}^\theta$.

3 Boundary Conditions

Boundary Conditions for 3DGE

There is an inherent difficulty in determining correct boundary conditions for the potentials in the vorticity-potential formulation. Any specified velocity on the boundaries does not imply unique scalar and vector potentials. A set of compatible restrictions on the potentials must be imposed. A discussion about the admissible boundary conditions for the potentials can be found in the work of [11,12] and [13].

The boundary conditions used for the 3DGE are summarized in Table 1 in which v_n^i, v_n^o are the mean normal inlet and outlet velocities and $\mathbf{E}$ is a vector defined on the inlet surface S that satisfies

$$\mathbf{E}\cdot\mathbf{t}_1 = 0, \quad \mathbf{E}\cdot\mathbf{t}_2 = 0, \quad \mathbf{n}\cdot[(\nabla_s \times (\nabla_s \times \mathbf{E})] = \mathbf{n}\cdot\mathbf{V} - v_n^i \tag{31}$$

In these equations, $\{\mathbf{n}, \mathbf{t}_1, \mathbf{t}_1\}$ is a local orthogonal coordinate system.

	Solid Wall	Inlet	Outlet
ϕ	$\frac{\partial \phi}{\partial n} = 0$	$\frac{\partial \phi}{\partial n} = v_h^i$	$\frac{\partial \phi}{\partial n} = v_n^0$
$\mathbf{A}$	$\mathbf{A} = 0$ $\nabla \cdot \mathbf{A} = 0$	$\mathbf{A} = \nabla_S \times E$ $\nabla \cdot \mathbf{A} = 0$	$\frac{\partial^2 \mathbf{A}}{\partial \mathbf{s}^2} = 0$
$\mathbf{W}$	$\mathbf{W} = (\nabla \times \mathbf{V})_{\text{Wall}}$	$\mathbf{W} = (\nabla \times \mathbf{V})_{\text{Inlet}}$	$\frac{\partial \mathbf{W}}{\partial \mathbf{s}} = 0$

Table 1: Boundary Conditions for 3DGE

Boundary Conditions for MPAGE

The boundary conditions for the modified passage-averaged equations (25–28) are summarized in Table 2 in which $\bar{v}_n^i$ and $\bar{v}_n^o$ are the average normal inlet and outlet velocities respectively.

4 Solution Procedure

The simulation of the rotor-stator flow interaction within a turbomachine consists of two sets of equations; the three-dimensional governing equations (3DGE) and the modified passage-averaged governing equations (MPAGE). The 3DGE are used within each blade region to provide the three-dimensional flow fields, while the MPAGE are used to link these flow fields in an average sense. The coupling between these two sets of equations and the data flow from each other will be described.

	Solid Wall	Inlet	Outlet
$\bar{\phi}$	$\frac{\partial \bar{\phi}}{\partial n} = 0$	$\frac{\partial \bar{\phi}}{\partial n} = \bar{v}_n^i$	$\frac{\partial \bar{\phi}}{\partial n} = \bar{v}_n^0$
$\bar{A}^\theta$	$\bar{A}^\theta = 0$	$\bar{A}^\theta = 0$	$\frac{\partial^2}{\partial s^2}(B\bar{A}^\theta) = 0$
$\bar{w}^\theta$	$B\bar{w}^\theta = \frac{\partial(B\bar{v}^r)}{\partial z} - \frac{\partial(B\bar{v}^z)}{\partial r}$	$B\bar{w}^\theta = \frac{\partial(B\bar{v}^r)}{\partial z} - \frac{\partial(B\bar{v}^z)}{\partial r}$	$\frac{\partial}{\partial s}(B\bar{w}^\theta) = 0$
$\bar{v}^\theta$	$\bar{v}^\theta = (\bar{v}^\theta)_{\text{wall}}$	$\bar{v}^\theta = \bar{v}_i^\theta$	$\frac{\partial}{\partial s}(B\bar{v}^\theta) = 0$

Table 2: Boundary Conditions for MPAGE

Data Flow from the 3DGE to the MPAGE

The passage-averaged equations (25–30) have the same form as the axisymmetric flow equations with the addition of external force terms which model the three-dimensional effects into the MPAGE.

Outside the blade passages, the flow is taken to be axisymmetric and these external force terms are zero. Within the blade passages, they are computed from the 3DGE solutions. Most of these terms use only the values of the 3DGE solutions on the pressure and suction surfaces, while some terms, like $\overline{\tilde{\mathbf{W}} \times \tilde{\mathbf{V}}}$ require integration of the 3DGE solutions across the blade passage. All these terms can be computed explicitly and the calculations can be performed outside the 3DGE and MPAGE solvers. The input data are the geometry parameters and the 3DGE solutions. The output data are the external force terms which are needed for solving the MPAGE.

Data Flow from the MPAGE to the 3DGE

From the formulation of the 3DGE, it is clear that in order to solve these equations, the only required information is the inlet velocity distribution.

To specify an accurate three-dimensional inlet velocity profile is very difficult and even impossible for a general configuration. However, in the present study, since the flow is taken to be axisymmetric outside the blade rows, the inflow conditions at the entrance of each blade row are also axisymmetric. The passage-averaged velocity can be used as inlet velocity profile. These inlet velocities are updated by the MPAGE solutions.

The data flow from the 3DGE to the MPAGE and vice versa is repeated until convergence is achieved.

5 Results

Description of the NEL Pump

The NEL pump is a mixed-flow machine with a five blades rotor and a nine blades stator. Details of the physical dimensions of the blades and a general description of the pump are given in [16].

The measurements reported by [17] were performed in an air model of the machine at a shaft speed 1200 r.p.m. of the rotor. The experimental data for all velocities are normalized by the blade velocity at the rotor trailing edge mid-point, which is $U_t = 27m/s$, corresponding to a Reynolds number of Re=1.5x10^6. However, since the present study is for laminar flow, the Reynolds number for the numerical computation, run at the best efficiency point of the pump, was set to 1500.

The meridional computational domain is shown in Figure 1, and is divided into five regions. The rotor is located from $s = 1$ to $s = 2$ and the stator from

$s = 3$ to $s = 4$. The inlet is at station $s = 0$ and the outlet at $s = 5$. It is noted that in the numerical simulation, the rotor tip clearance was not considered.

A grid of 13x59 was used for the MPAGE computation with 13 points in the radial direction. There were 15 points spaced uniformly in the circumferential direction for the rotor and 13 points for the stator.

Rotor Three-Dimensional Results

For comparison of the numerical predictions with the experimental measurements of [17], the results are presented in terms of the velocity component parallel to the streamwise grid line, V_p, the tangential velocity component in the relative rotating frame of reference, W_t and the velocity component normal to the streamwise grid line, V_n.

Figures 2 to 4 show the blade-to-blade velocity variations from the suction side "SS" to the pressure side "PS" and from hub-to-shroud. Also to show, in these figures, the streamwise evolution of the velocity components within the rotor, the blade-to-blade variations are given near the rotor inlet (s=1.07), at mid-chord (s=1.5) and near the rotor outlet (s=1.87). On these figures, the blade-to-blade graphs are numbered from 3 to 12 corresponding to the normalized hub-to-shroud distance R=0.167, 0.333, 0.5, 0.667, 0.833 and 0.917 and detailed in [17].

Due to the change of the rotor geometry, the velocity component V_p (Figure 2) is accelerated near the blade suction surface in the mainstream flow region (R < 0.833). In the same region, the relative tangential component W_t (Figure 3) is decelerated near the suction surface and accelerated near the pressure surface. These observations agree well with the experimental data except at the edge of the blade surface boundary layers where the velocities are relatively higher than the measured ones. This is as expected since the Reynolds number for the

computation is a thousand times lower than the experimental one. Consequently, a thicker boundary layer on the blade surface is observed which induces higher velocities at the edge of the boundary layer.

In the near shroud region, $0.833 < R < 1.0$, complex turbomachinery flow phenomena are encountered. The blade boundary layers, the shroud boundary layer, the effects of the relative motion of the shroud and the associated secondary flow interacts to generate rapid changes in the flow pattern. It is evident that there is a discrepancy between the predictions and the measurements for velocity components V_p and W_t shown in Figs. 2 and 3.

The main reason for such a discrepancy is probably the absence of the blade-tip gap in the present numerical modeling. When the flow proceeds downstream, the tip leakage flow meet and interact with blade and shroud boundary layers, giving rise to a mixing region. Without the tip leakage flow, the shroud boundary layer will play an important and more dominant role in the outer annular region. Indeed, the numerical predictions in Figs. 2 and 3 show that, the flow close to the suction surface is decelerated, while near the pressure surface, the flow is accelerated by the moving shroud.

MPAGE Results without Stator

It is interesting to conduct a test to isolate the effect of the stator. This can be done by imposing all the external force terms to zero within the stator passage while keeping them within the rotor passage. In other words, the presence of the stator is totally neglected. For this pump, the function of the stator is to convert kinetic energy into pressure. Since the flow is incompressible, this energy is taken from the swirl component, W_t, of the velocity field generated by the rotor. In the absence of the stator, W_t, at the exit, is expected to be larger than with the stator. Indeed, this result is supported by the present numerical

prediction shown in Figure 5. It is observed that the velocity component V_p has no significant change (since the flow must conserve the mass across the blade section), while the velocity component W_t is dramatically decreased by the presence of the stator as the flow develops downstream.

6 Conclusions

A mathematical model for rotor-stator flow interaction simulation has been proposed. This model is based upon the passage-averaged vorticity-potential formulation to link the three-dimensional flow fields within the rotor and stator passages. In the passage-averaged equations, the presence of the blades is accounted for by force terms whose values are deduced from the three-dimensional flow fields. This procedure requires some iterations between the passage-averaged solutions and the three-dimensional solutions to achieve a convergent flow field. With regard to computer resources, this approach has many advantages:

(i) It avoids a full three-dimensional time dependent computation through a complete turbomachine.

(ii) It does not require the interpolation between the rotor moving grid and the stator stationary grid.

(iii) The external forces from the three-dimensional computations are more accurate than the forces from an approximate blade-to-blade computation.

(iv) It links the three-dimensional flow fields of the rotor and stator in an averaged sense.

The proposed model has been applied successfully to a mixed-flow pump and the predicted solutions were compared with the experimental data. Considering the absence of a proper turbulence model, the numerical results are reasonable and correctly represent the complex three-dimensional flow.

7 Acknowledgments

This work was supported by the National Science and Engineering Research Council of Canada (NSERC) and by the Centre de Recherche Informatique de Montréal (CRIM) and Institut de Recherche et Etude du Hydro-Québec (IREQ).

References

[1] Wu,C.H. (1952), A general theory of three-dimensional flow in subsonic and supersonic turbomachines of axial, radial and mixed-flow types, NACA TN 2604.

[2] Krimerman,Y. and Adler,D. (1978), The complete three-dimensional calculation of the compressible flow field in turbo impellers, J. Mech. Eng. Sci., 20, pp.149-158. 24, pp.389-415.

[3] Wang,Q.H., Zhu,G.X. and Wu,C.H. (1985), Quasi-three-dimensional and full three-dimensional rotational flow calculations in turbomachines, J. Eng. Gas Turbines and Power, ASME, 107, pp.277-285.

[4] Jennions,I.K. and Stow,P. (1985), A quasi-three-dimensional turbomachinery blade design system: part I - throughflow analysis, and part II - computerized system, J. Eng. Gas Turbines and power, ASME, 107, pp.301-316.

[5] Bosman,C. and Marsh,H. (1974), An improved method for calculating the flow in turbomachines including a consistent loss model, J. Mech. Eng. Sci., 16, pp.25-31.

[6] Bosman,C. and El Shaarawi,M.A.I. (1977), Quasi three-dimensional numerical solution of flow in turbomachines, J. Fluid Eng., ASME, 99, pp.132-140.

[7] Adamczyk,J.J. (1984), Model equation for simulating flows in multistage turbomachinery, NASA TM 86869.

[8] Adamczyk,J.J., Mulac,R.A. and Celestina,M.L. (1986), A model for closing the inviscid form of the average-passage equations system, J. Turbomachines, ASME, 108, pp180-186.

[9] Celestina,M.L., Mulac,R.A. and Adamczyk,J.J. (1986), A numerical simulation of the inviscid flow through a counterrotating propeller, J. Turbomachines, ASME, 108, pp.187-193.

[10] Adamczyk,J.J., Celestina,M.L., Beach,T.A. and Barnett,M (1990), Simulation of three-dimensional viscous flow within a multistage turbine, J. Turbomachines, ASME, 112, pp370-376.

[11] Hirasaki,G.J. and Hellums,J.D. (1970), Boundary conditions on the vector and scalar potentials in viscous three-dimensional hydrodynamics, Quart. Appl. Math., 28, pp.293-296.

[12] Wong,A.k. and Reize,J.A. (1984), An effective vorticity-vector potential formulation for the numerical solutions of three-dimensional duct flow problems, J. Comp. Phys., 55, pp.98-114.

[13] Yang H.R. and Camarero R. (1991), Internal three-dimensional viscous flow solutions using the vorticity-potential method, Int. J. Numer. Meth. Fluids, 12, pp.1-15.

[14] Roache,P.J. (1982), Computational fluid dynamics, Hermosa Publishers.

[15] Aziz,K. and Hellums,J.D. (1967), Numerical solution of the three-dimensional equations of motion for laminar nature convection, Phys. Fluids, 10, pp.314-325.

[16] Carey,C., Fraser,S.M., Rachman,D. and Wilson,G. (1985a), Studies of the flow of air in a model mixed-flow pump using laser doppler anemometry, Part 1: Research facility and instrumentation, NEL Report 698.

[17] Carey,C., Fraser,S.M., Rachman,D. and Wilson,G. (1985b), Studies of the flow of air in a model mixed-flow pump using laser doppler anemometry, Part 2: Velocity measurements within the impeller, NEL Report 699.

Appendix

The External forces for the modified passage-averaged equations are

$$
\begin{aligned}
F_w^\theta \;=\; & \frac{1}{Re\;k}\quad [\frac{1}{r}\frac{\partial}{\partial\theta}(\nabla\lambda_s\cdot\mathbf{W}_s-\nabla\lambda_p\cdot\mathbf{W}_p)] \\
& -[\frac{\partial}{\partial z}(\frac{1}{r}(\frac{\partial\lambda_s}{\partial\theta}w_s^z-\frac{\partial\lambda_p}{\partial\theta}w_p^z)-(\frac{\partial\lambda_s}{\partial\theta}w_s^\theta-\frac{\partial\lambda_p}{\partial\theta}w_p^\theta)) \\
& -\frac{\partial}{\partial r}((\frac{\partial\lambda_s}{\partial r}w_s^\theta-\frac{\partial\lambda_p}{\partial r}w_p^\theta)-\frac{1}{r}(\frac{\partial\lambda_s}{\partial\theta}w_s^r-\frac{\partial\lambda_p}{\partial\theta}w_p^r))] \\
& -[(\frac{\partial\lambda_s}{\partial z}(\frac{1}{r}\frac{\partial w^z}{\partial\theta}-\frac{\partial w^\theta}{\partial z})_s-\frac{\partial\lambda_p}{\partial z}(\frac{1}{r}\frac{\partial w^z}{\partial\theta}-\frac{\partial w^\theta}{\partial z})_p) \\
& -(\frac{\partial\lambda_s}{\partial r}(\frac{1}{r}w^\theta-\frac{\partial w^\theta}{\partial r}-\frac{1}{r}\frac{\partial w^r}{\partial\theta})_s \\
& -\frac{\partial\lambda_p}{\partial r}(\frac{1}{r}w^\theta-\frac{\partial w^\theta}{\partial r}-\frac{1}{r}\frac{\partial w^r}{\partial\theta})_p)] \\
& -\frac{1}{k}\quad {}^n\bar{v}^\theta[\nabla\lambda_s\cdot\mathbf{W}_s-\nabla\lambda_p\cdot\mathbf{W}_p] \\
& -r\omega[(\frac{\partial\lambda_s}{\partial z}w_s^z-\frac{\partial\lambda_p}{\partial z}w_p^z)+(\frac{\partial\lambda_s}{\partial r}w_s^r-\frac{\partial\lambda_p}{\partial r}w_p^r)] \\
& -\quad \frac{\partial}{\partial z}(B\overline{\tilde{w}^\theta\tilde{v}^z}-B\overline{\tilde{w}^z\tilde{v}^\theta})-\frac{\partial}{\partial r}(B\overline{\tilde{w}^r\tilde{v}^\theta}-B\overline{\tilde{w}^\theta\tilde{v}^r}) \\
& -\bar{w}^\theta[\frac{\partial B}{\partial r}\bar{v}^r+\frac{\partial B}{\partial z}\bar{v}^z] \\
& +\quad [\frac{\partial(B\bar{v}^\theta)}{\partial r}+\frac{1}{r}B\bar{v}^\theta-\frac{r\omega}{k}(\frac{\partial\lambda_s}{\partial z}-\frac{\partial\lambda_p}{\partial z})]\frac{\partial\bar{v}^\theta}{\partial z} \\
& -[\frac{\partial(B\bar{v}^\theta)}{\partial z}+\frac{r\omega}{k}(\frac{\partial\lambda_s}{\partial z}-\frac{\partial\lambda_p}{\partial z})]\frac{\partial\bar{v}^\theta}{\partial r} \\
& +\frac{r\omega}{k}(\frac{\partial\lambda_s}{\partial z}-\frac{\partial\lambda_p}{\partial z})(\frac{1}{r}\bar{v}^\theta)
\end{aligned}
\tag{32}
$$

$$
\begin{aligned}
F_A^\theta &= -\frac{1}{k} \quad [\frac{1}{r}\frac{\partial}{\partial\theta}(\nabla\lambda_s\cdot\mathbf{A}_s - \nabla\lambda_p\cdot\mathbf{A}_p)] \\
&\quad + [(\frac{\partial\lambda_s}{\partial z}(\frac{1}{r}\frac{\partial A^z}{\partial\theta} - \frac{\partial A^\theta}{\partial z})_s - \frac{\partial\lambda_p}{\partial z}(\frac{1}{r}\frac{\partial A^z}{\partial\theta} - \frac{\partial A^\theta}{\partial z})_p] \\
&\quad - [\frac{\partial\lambda_s}{\partial r}(\frac{1}{r}A^\theta - \frac{\partial A^\theta}{\partial r} - \frac{1}{r}\frac{\partial A^r}{\partial\theta})_s \\
&\quad - \frac{\partial\lambda_p}{\partial r}(\frac{1}{r}A^\theta - \frac{\partial A^\theta}{\partial r} - \frac{1}{r}\frac{\partial A^r}{\partial\theta})_p]
\end{aligned} \tag{33}
$$

$$
\begin{aligned}
F_v^\theta &= \frac{1}{Re\ k} \quad [\frac{\partial\lambda_s}{\partial r}((\frac{\partial v^\theta}{\partial r})_s - \frac{1}{r}v_s^\theta) - \frac{\partial\lambda_s}{\partial r}((\frac{\partial v^\theta}{\partial r})_s - \frac{1}{r}v_s^\theta)] \\
&\quad + \frac{1}{r}[\frac{\partial\lambda_s}{\partial\theta}(\frac{\partial v^\theta}{\partial\theta})_s - \frac{\partial\lambda_p}{\partial\theta}(\frac{\partial v^\theta}{\partial\theta})_p] \\
&\quad + [\frac{\partial\lambda_s}{\partial z}(\frac{\partial v^\theta}{\partial z})_s - \frac{\partial\lambda_p}{\partial z}(\frac{\partial v^\theta}{\partial z})_p] \\
&\quad + r\omega[\frac{\partial}{\partial r}(\frac{\partial\lambda_s}{\partial r} - \frac{\partial\lambda_p}{\partial r}) - \frac{\partial}{\partial z}(\frac{\partial\lambda_s}{\partial z} - \frac{\partial\lambda_p}{\partial z})] \\
&- \quad \frac{2}{r}B\overline{\tilde{v}^r\tilde{v}^\theta} + \frac{\partial}{\partial r}(B\overline{\tilde{v}^r\tilde{v}^\theta}) + \frac{\partial}{\partial z}(B\overline{\tilde{v}^z\tilde{v}^\theta}) \\
&\quad - \bar{v}^\theta[\frac{\partial B}{\partial r}\bar{v}^r + \frac{\partial B}{\partial z}\bar{v}^z] \quad + \quad B\overline{D_p}
\end{aligned} \tag{34}
$$

$$
F_\phi = -\frac{1}{k}\nabla\cdot(\phi_s\nabla\lambda_s - \phi_p\nabla\lambda_p) \tag{35}
$$

$$
F_v^r = -\frac{1}{k}(\frac{\partial\lambda_s}{\partial r}\phi_s - \frac{\partial\lambda_p}{\partial r}\phi_p) \tag{36}
$$

$$
F_v^z = -\frac{1}{k}(\frac{\partial\lambda_s}{\partial z}\phi_s - \frac{\partial\lambda_p}{\partial z}\phi_p) \tag{37}
$$

with

$$
\begin{aligned}
D_p &= \frac{1}{Re}[\frac{\partial}{\partial r}(\frac{1}{r}\frac{\partial v^\theta}{\partial r}) + \frac{\partial^2 v^\theta}{\partial z^2}] \\
&\quad -[\frac{1}{r}\frac{\partial}{\partial r}(rv^rv^\theta) + \frac{\partial}{\partial z}(v^zv^\theta) + \frac{1}{r}v^rv^\theta]
\end{aligned} \tag{38}
$$

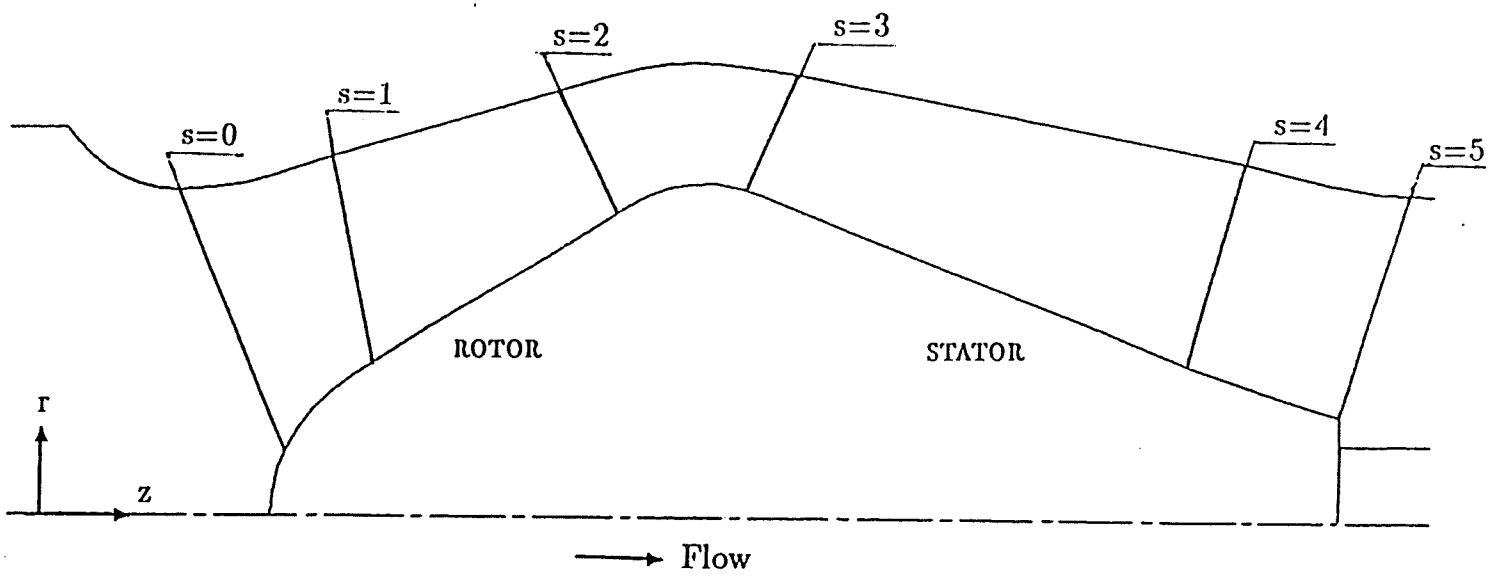

Figure 1: Domain for the MPAGE Computation

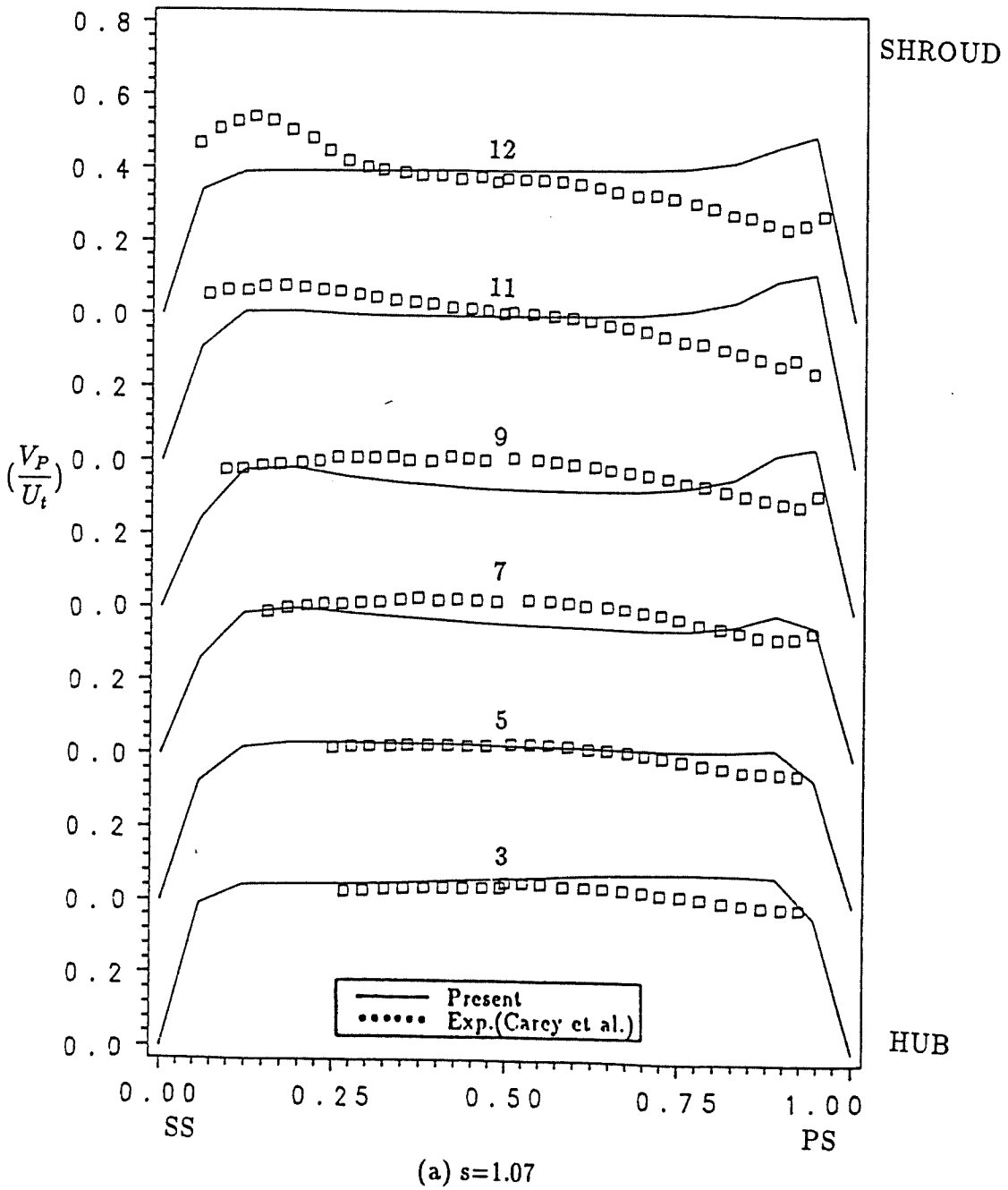

(a) s=1.07

Figure 2: Blade-to-Blade Velocity Components V_p, Rotor

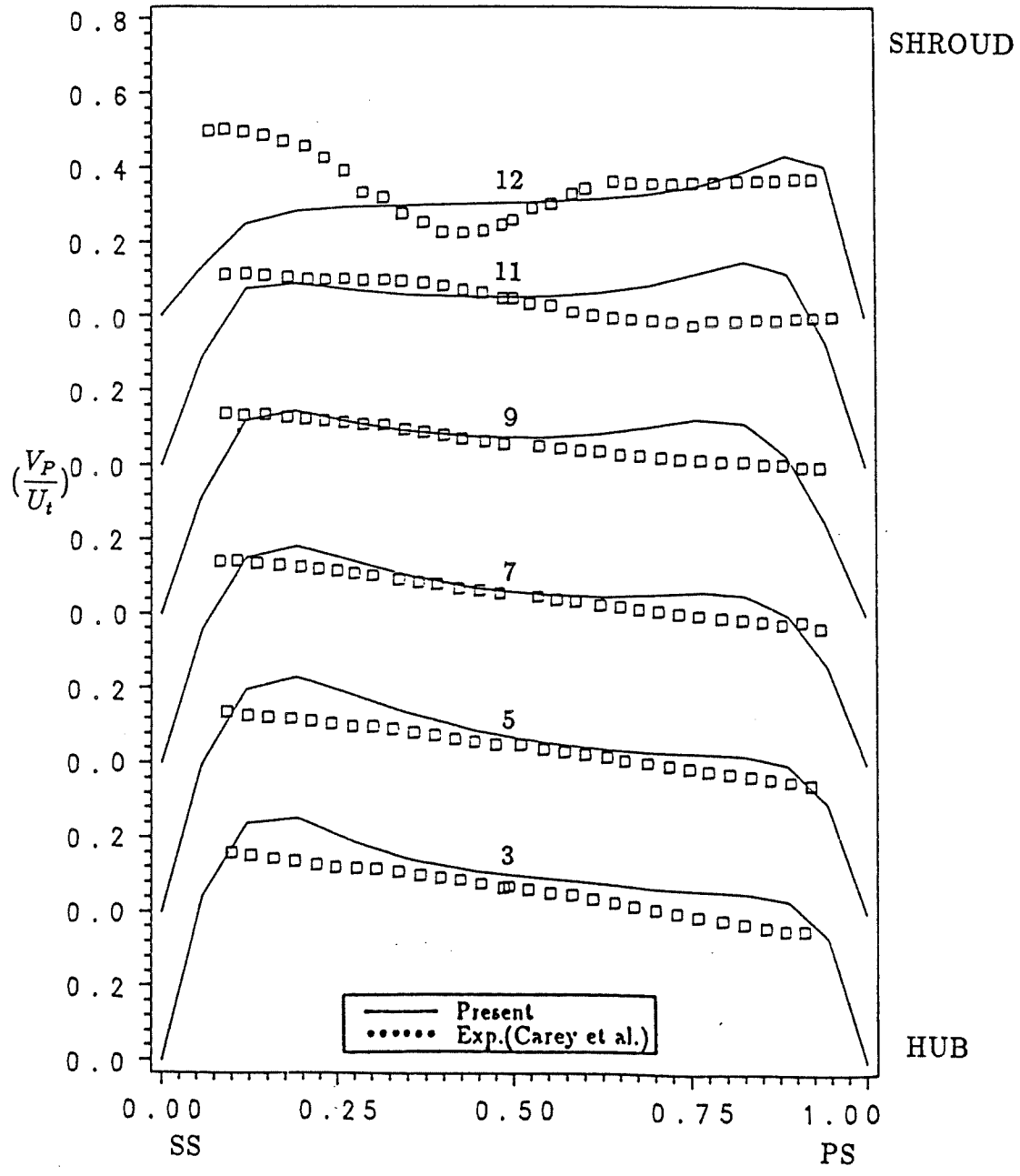

(b) s=1.50

Figure 2: Blade-to-Blade Velocity Components V_p, Rotor

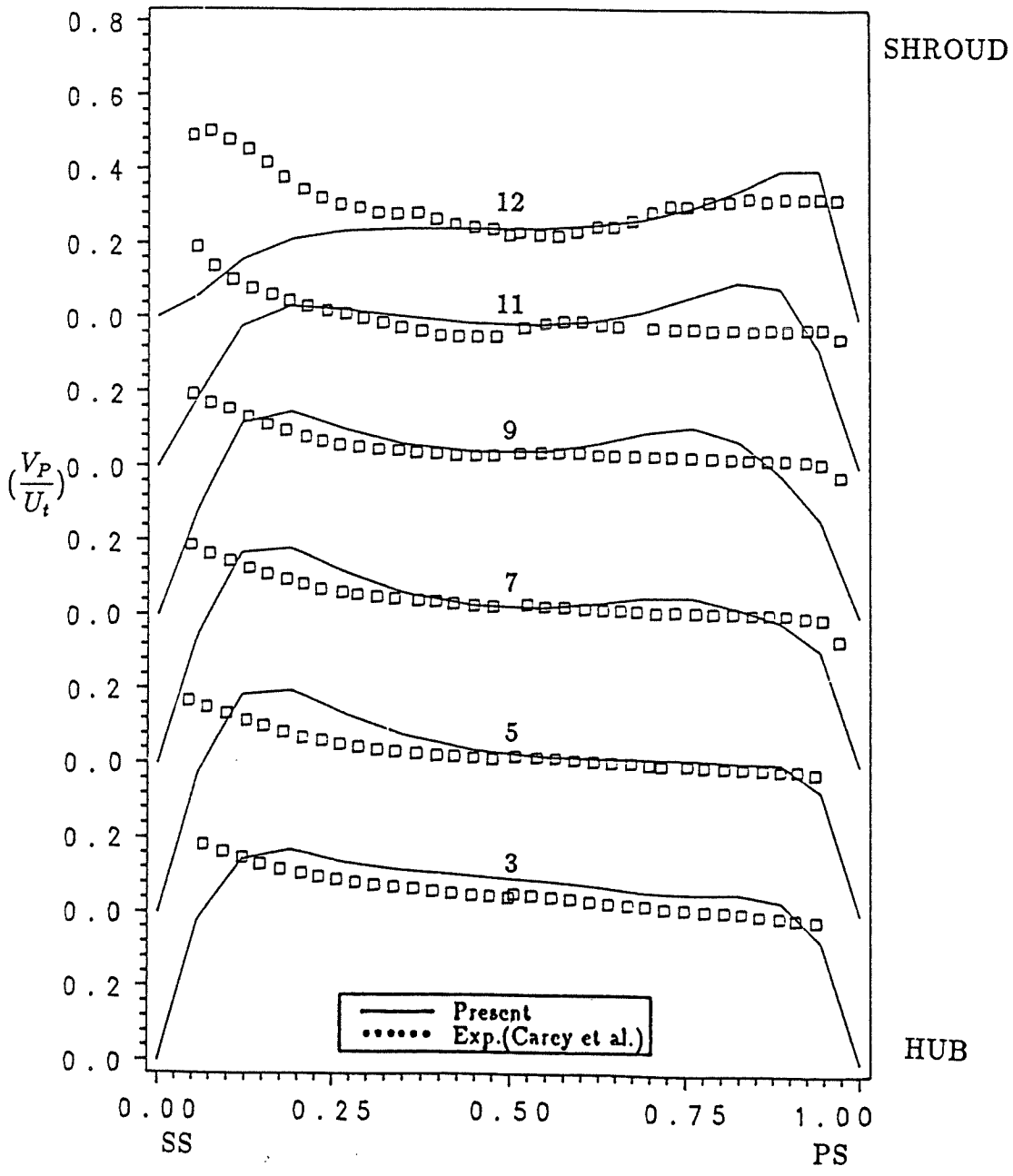

(c) s=1.86

Figure 2: Blade-to-Blade Velocity Components V_p, Rotor

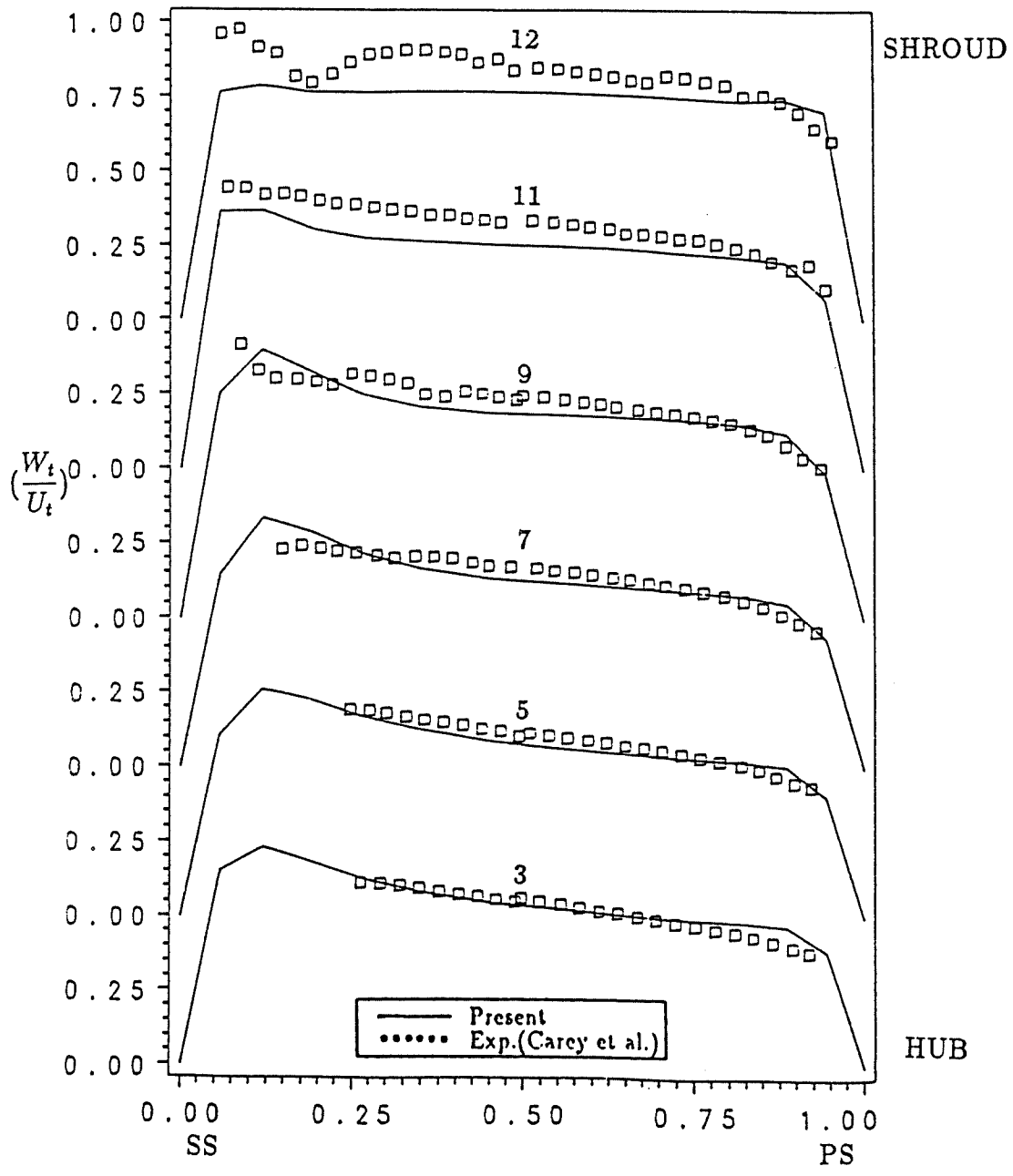

(a) s=1.07

Figure 3: Blade-to-Blade Velocity Components W_t, Rotor

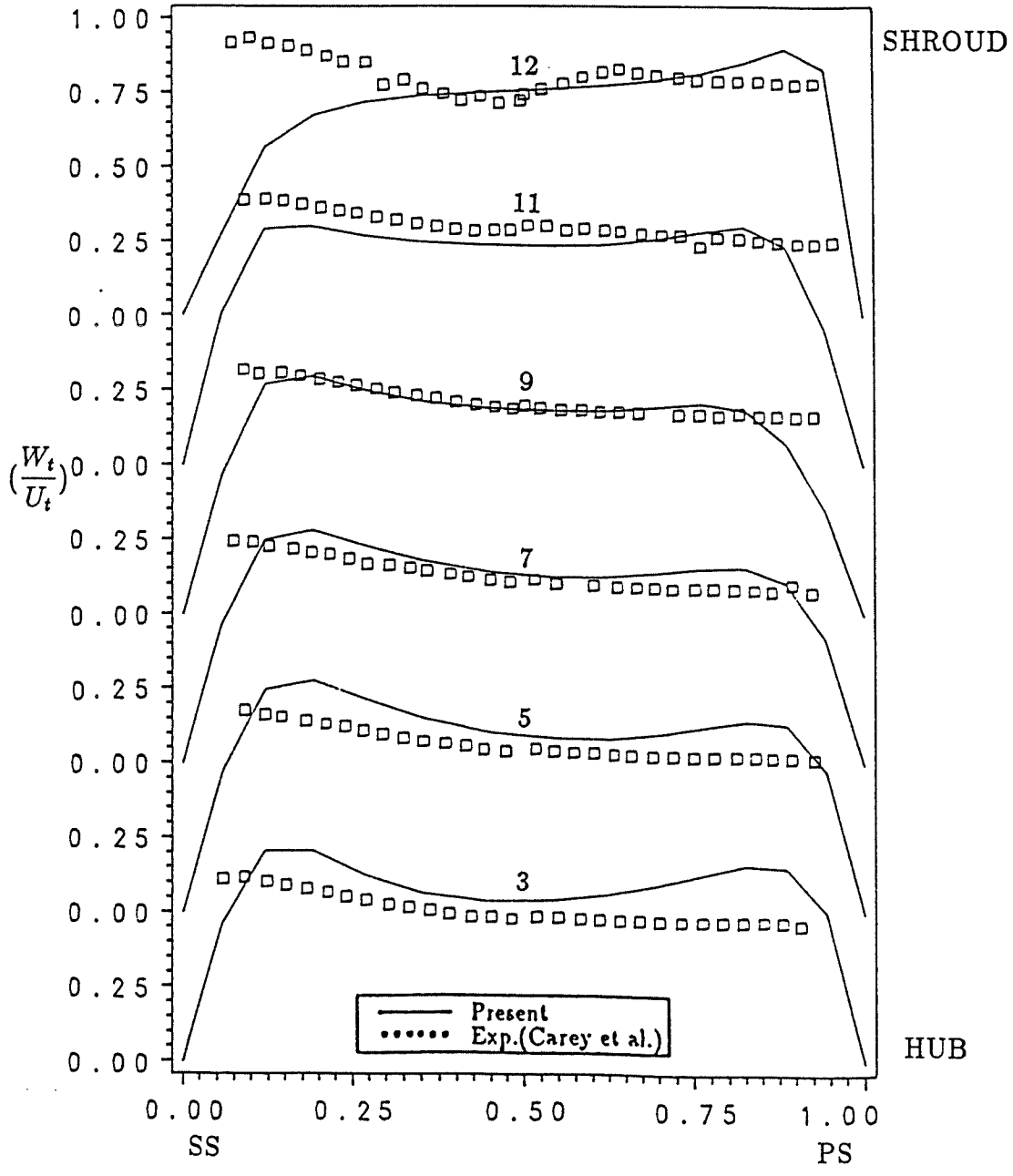

(b) s=1.50

Figure 3: Blade-to-Blade Velocity Components W_t, Rotor

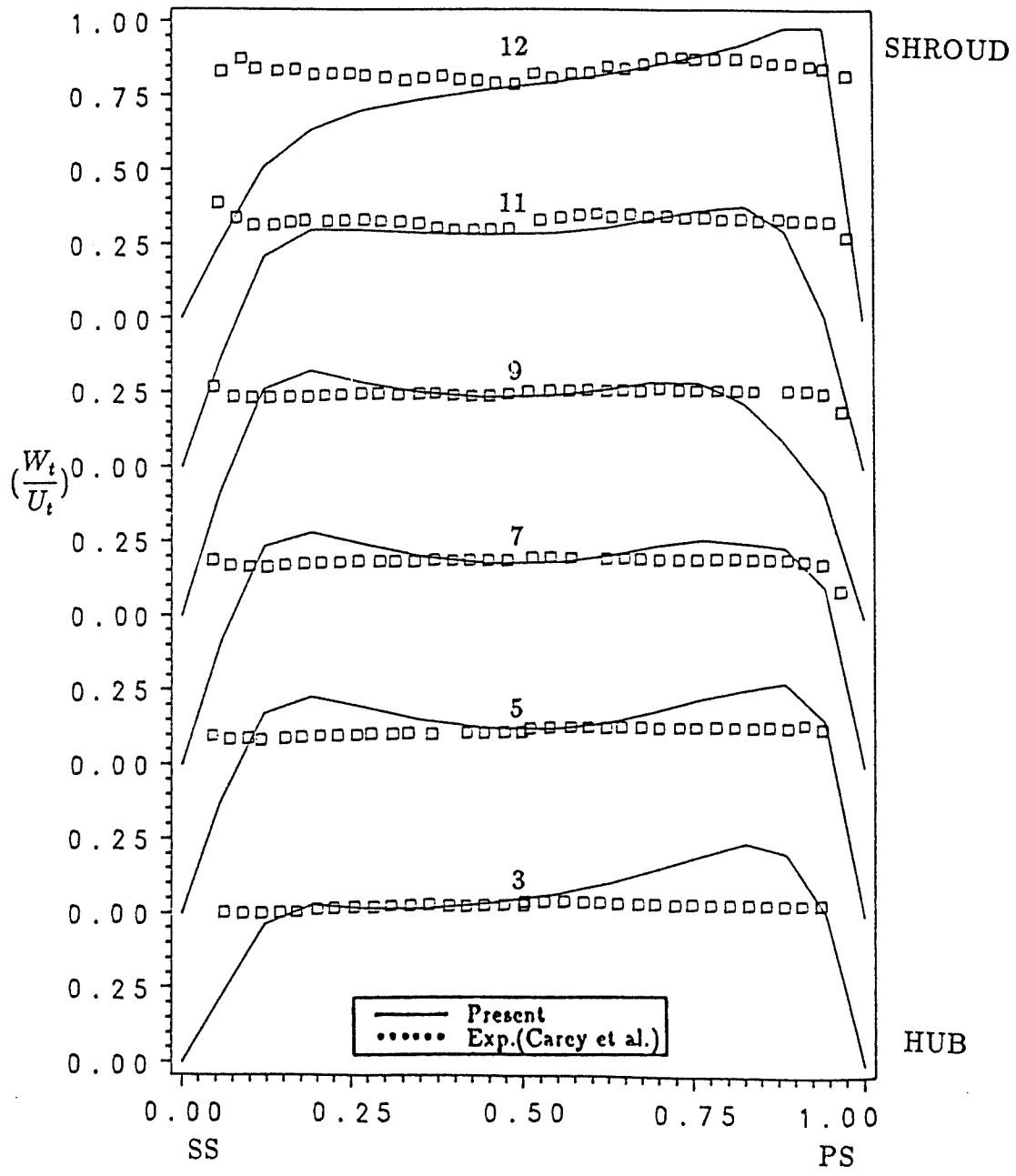

(c) s=1.86

Figure 3: Blade-to-Blade Velocity Components W_t, Rotor

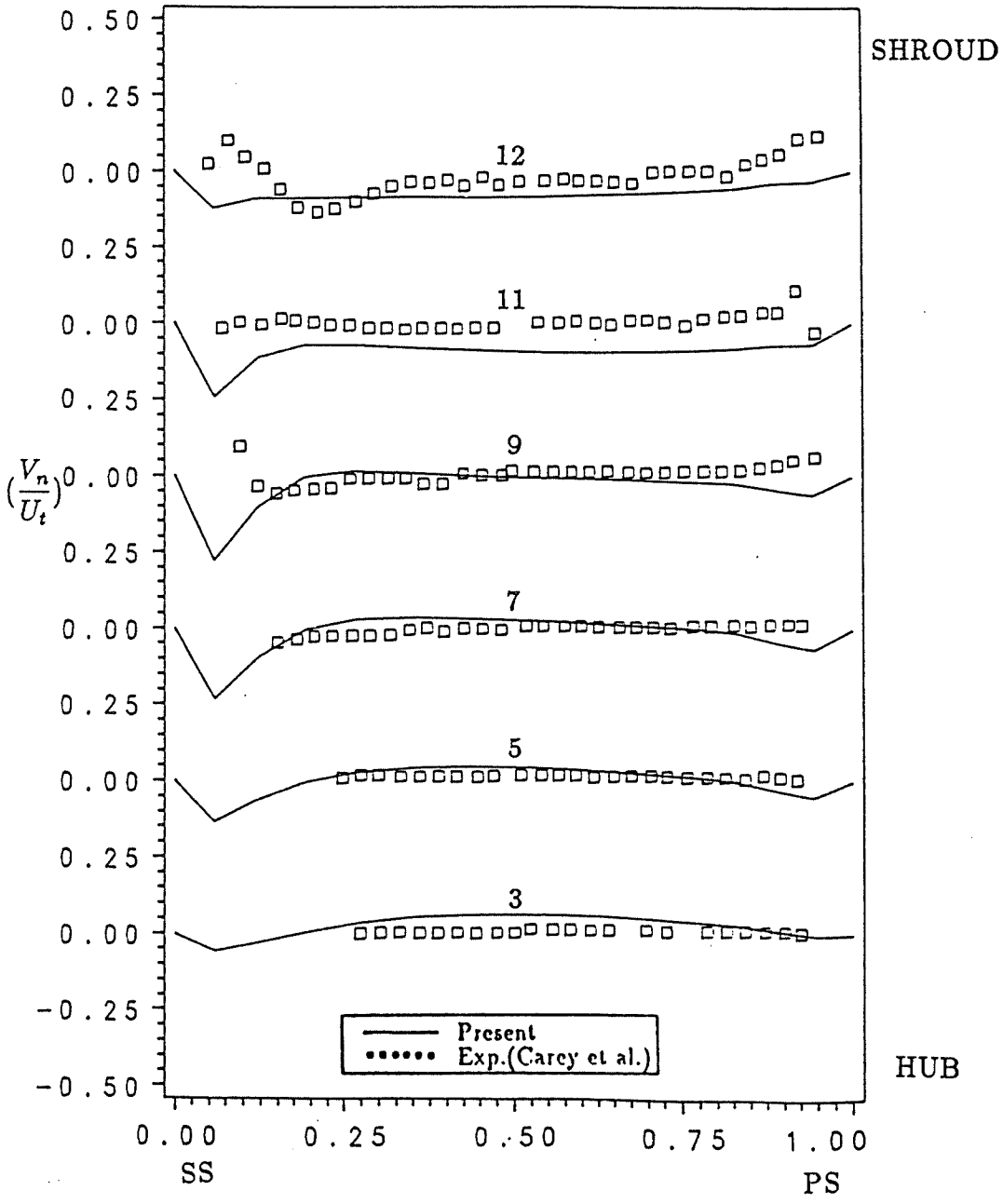

(a) s=1.07

Figure 4: Blade-to-Blade Velocity Components V_n, Rotor

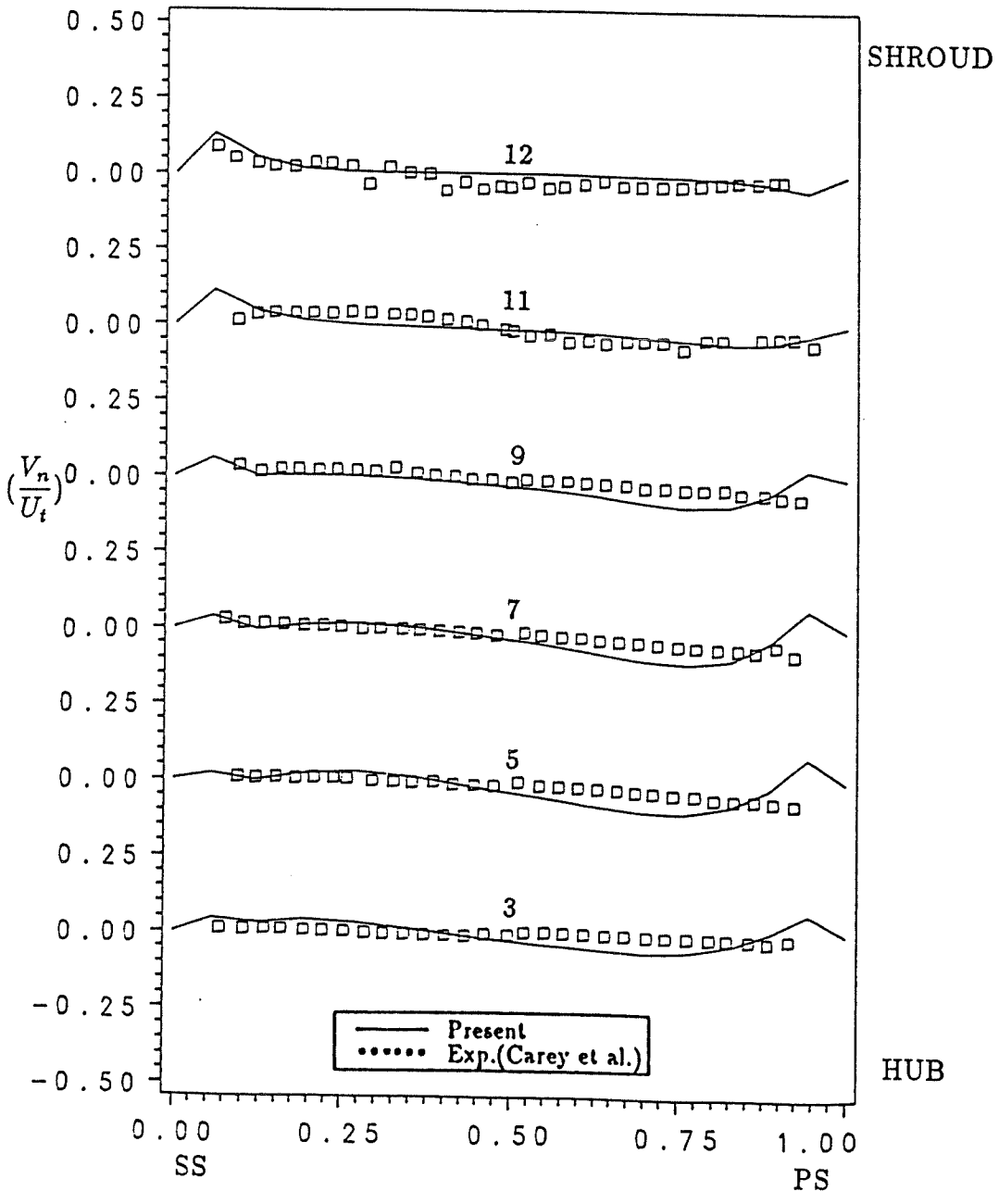

(b) s=1.50

Figure 4: Blade-to-Blade Velocity Components V_n, Rotor

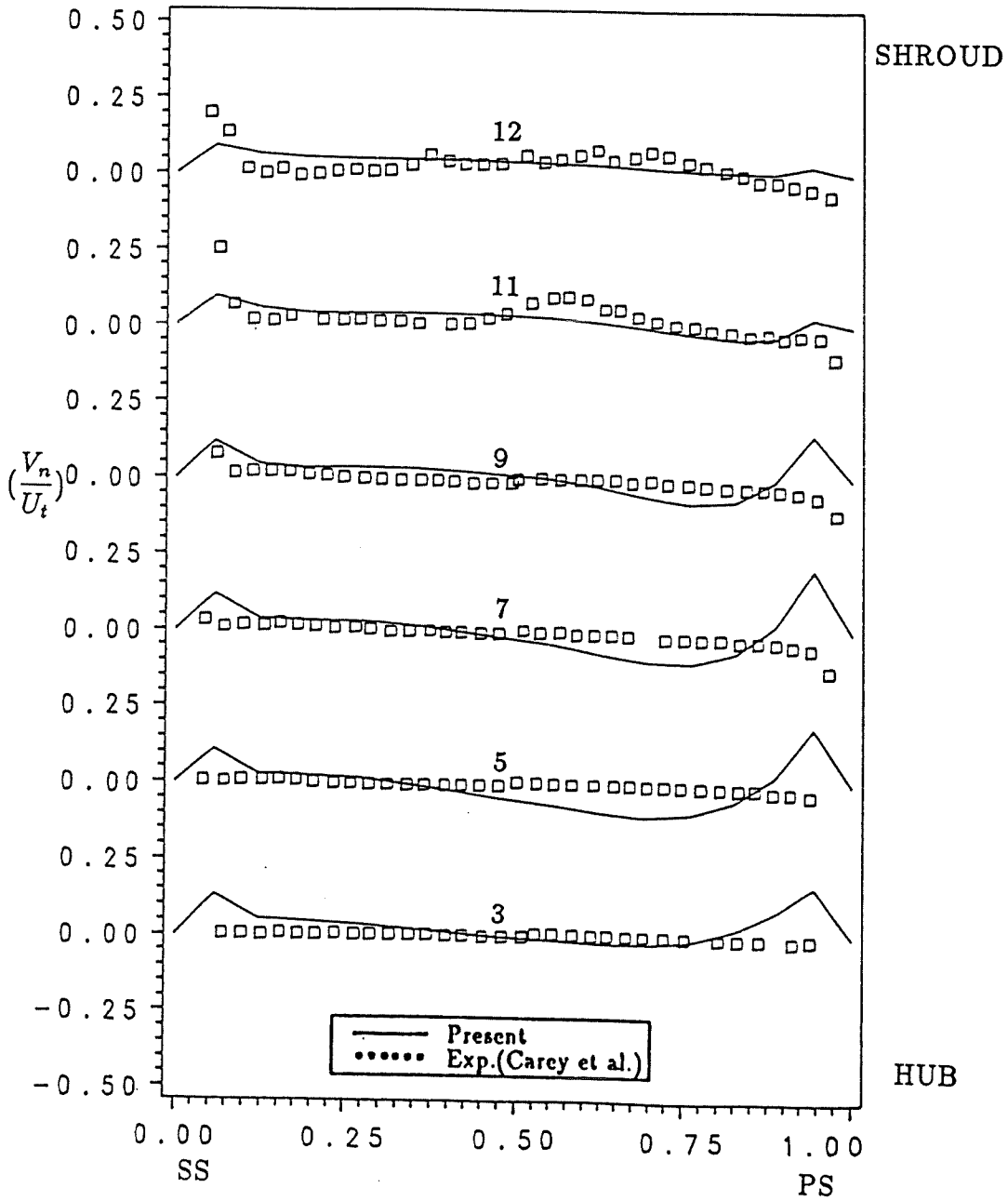

(c) s=1.86

Figure 4: Blade-to-Blade Velocity Components V_n, Rotor

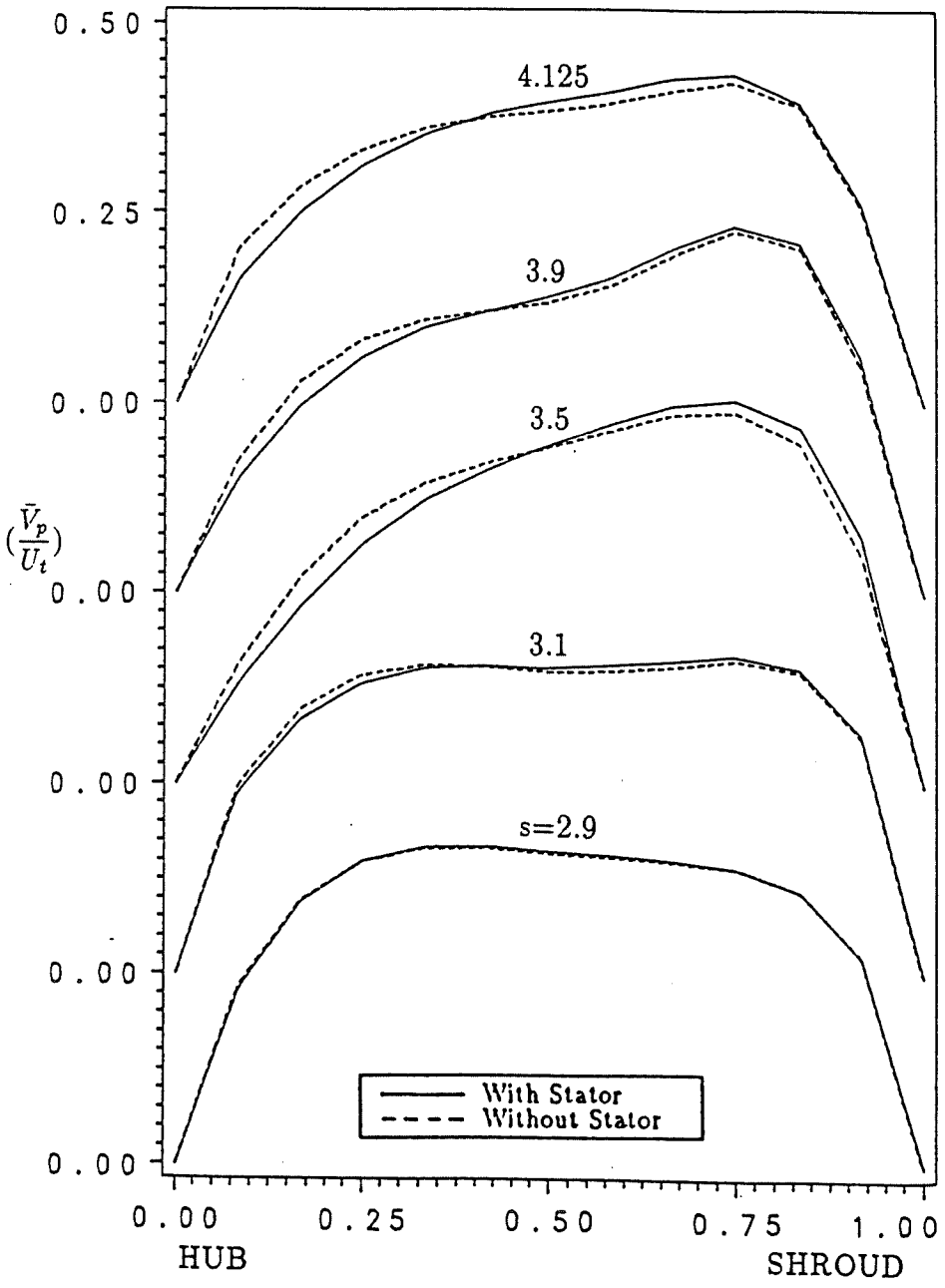

(a) Component $\bar{V}_p$

Figure 5: Passage-Averaged Hub-to-Shroud Velocities with and without the Stator

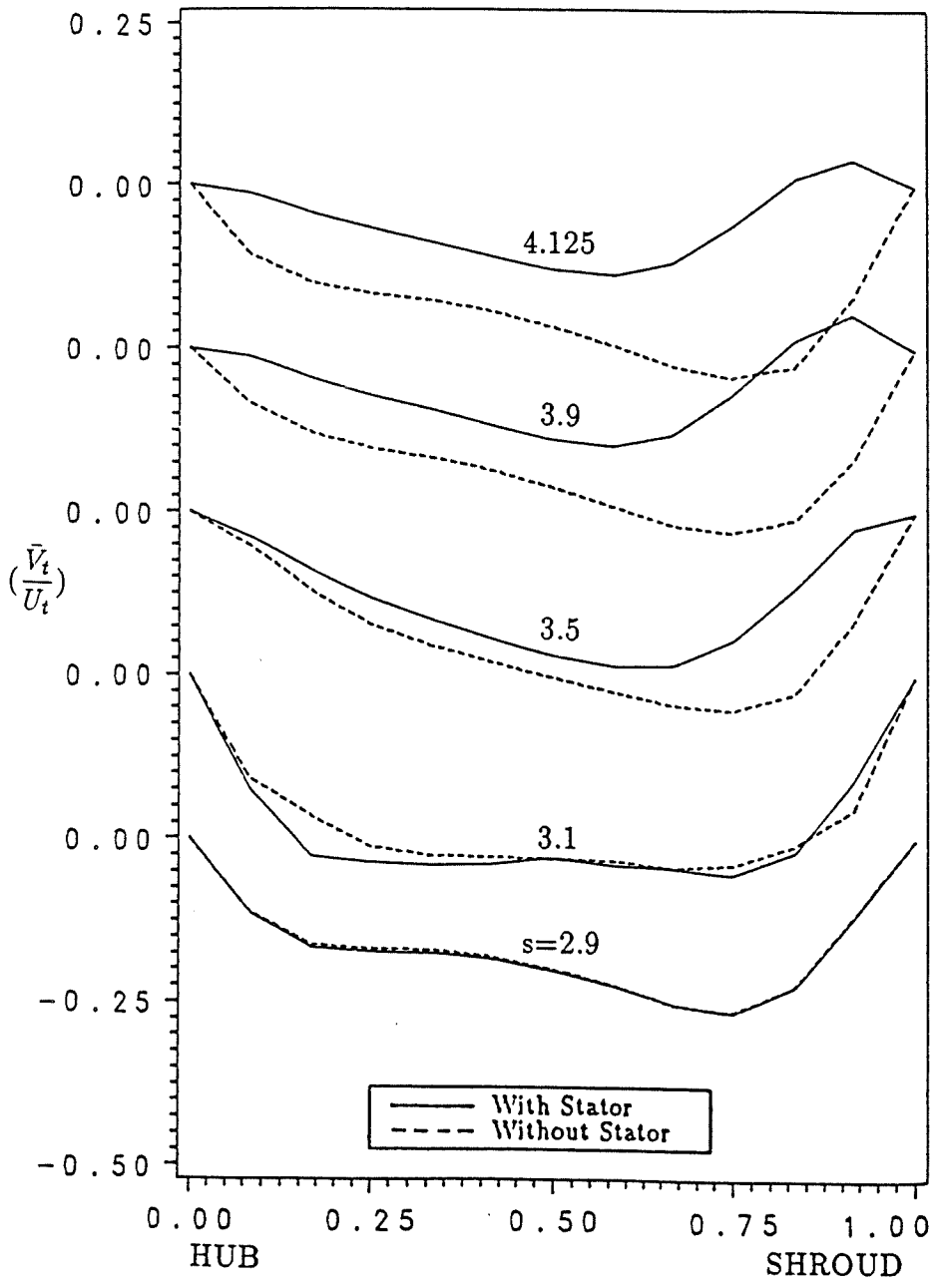

(b) Component $\bar{V}_t$

Figure 5: Passage-Averaged Hub-to-Shroud Velocities with and without the Stator